A

Synopsis report

of

Ph.D. Dissertation

Phase transformations in interstitial-free, and low density steels

Submitted By

Mrinmoy Sinha
(14921006)

Supervisor

Dr. Sadhan Ghosh

Assistant Professor, Department of Metallurgical and Materials Engineering, IIT Roorkee

DEPARTMENT OF METALLURGICAL AND MATERIALS ENGINEERING
INDIAN INSTITUTE OF TECHNOLOGY ROORKEE
ROORKEE - 247667 (INDIA)

August, 2019

Abstract:

The interstitial-free (IF) steel is extremely soft and ductile. The strengthening is the key focus of the present study by heat treatment. The samples have been soaked in the austenitic temperature domain followed by different rates of cooling (furnace cooling, air cooling and water quenching) in a Gleeble 3800® thermo-mechanical simulator. The outcome exhibits a dramatic improvement in strength as compared to reported conventional techniques. The electron microscopy along with EBSD has characterized lath martensite in this commercial grade steel. The hot deformation of austenite to martensite has also been investigated to study constraints in the martensite formation with variant selection in the present alloy system as well for a comparative study. The structure-property correlation is the key ingredient to address the role of the hierarchical structure (block and sub-block boundaries) against microstructural morphology for the obtained mechanical properties.

In the additional part of the present work, some calculation with Dictra simulation has been performed to study phase transformations in low density steel. It is known that Al as the alloying element is inevitable for density reduction of steels. It in turns produces δ-ferrite in the system. The consequence of δ-ferrite to the austenite formation is the key theme in this part of work.

1.1 Background and motivation

Interstitial free steel: The applications of interstitial free (IF) steel are burgeoning, since its commercial production in the 1980s. The steel is used regularly for the outer shells of cars, beverage cans, refrigerator enclosure, enamel wares, and house hold appliances etc. The primary reason is the extremely high formability. The interstitial elements like carbon and nitrogen in this steel are present in a trace quantity (30-40 ppm), and those are further scavenged by Ti and Nb during alloying. The substitutional elements, in general, are also very low. The alloy chemistry thus makes the steel softer than even low carbon steel and less resistant to denting. From time to time, various researchers have intended to address this issue via grain refining, bake hardening, solid solution strengthening, precipitation hardening etc. Despite these, strengthening still remains a key issue in the current perspective. In the present work, microstructure modification by heat treatment has been explored to impart strengthening as the novel approach. Hot deformation is the established technique in steel metallurgy. Without hot rolling and hot stamping, finishing the end products of steels is difficult. The process involves mechanical deformation and phase transformations simultaneously, as also a part of the present study.

Low density steel: Steel is an evergreen structural material, though its dominance has been slipping in recent years as engineers seek to find lighter components. As the issue is weight, steel is heavy because it is made mostly out of iron with a density (ρ) 7.8 gm/cm³. Adding a lighter element like Al (ρ =2.7 gm/cm³) of 1wt.% leads to a density reduction of roughly 1.3%. The steel researchers have felt that this may be good enough to renew its competitiveness in mass transports, while countering stringent pollution norms against the CO_2 emission. The concept sounds simple, but the underlying metallurgical issues are not that straight forward. As a major consequence, the excessive use of aluminium leads to the formation of δ-ferrite in a large fraction; as an example, 9 wt.% aluminium corresponds to ~60% δ-ferrite in the current system from the liquid phase. This trend is quite unusual and unforeseen in other steel systems. Thus, the present work would like to study its influence in the microstructure build up during solidification-casting

1.2 Defining problems based on the research gap

Interstitial free steel: An extensive literature survey has been carried out on techniques for strengthening of interstitial-free steels and ultra-low carbon steels with merits and demerits. On the important findings from the literature and research papers, the following research gaps have been identified to formulate the problems for the present study.

(a) *Martensitic transformation in commercial IF steel by water quenching*:

Until now martensitic transformation by water quenching has been seen in ultra-low carbon steels alloyed with high concentration of austenite stabilizers or boron addition. Hence forth they are different than commercial IF steels. The martensitic transformation in commercial IF steel has been reported by hydrostatic pressure where explanation is still lacking. Therefore, the present work would like to perform strengthening through phase transformation to state the challenges of obtaining martensite in IF steel additionally.

(b) *Mechanical property in lieu of martensite in IF steel*:

IF steel is known to have extremely high formability. It has a drawback of strengthening. Until now there is no mechanical property co-relation data available on strengthening of IF steel by martensitic transformation as an integral part of the present study.

(c) *Martensite in deformed versus undeformed austenite*:

The extent of prior deformation to the martensitic transformation will be investigated with reference to the water quenched sample. In an IF steel, such investigation is rare to understand the phase transformation in details.

Low density steel: Aluminium is the key ingredient in low density steels. It leads to the formation of δ-ferrite in a large fraction. The role of δ-ferrite to the austenite formation and the subsequent phase transformation has not been explored earlier, until in the present work.

For the sake of simplicity, the outcome from the research work of ***Interstitial free steel*** and ***Low density steel*** will be discussed separately, chapter wise in different sections.

1.3 sample details and related techniques → IF steel

The samples have been originally received from TATA Steel, Jamshedpur, India with a commercial-purity claimed to be 99.3% on a weight basis. The chemical composition is given in Table 1, as confirmed by optical emission spectroscopy in wt%. Thermodynamic prediction of the phase stability has been carried out using *Thermo-calc* software with the *TCFE7* database and the *SGTE* module. The ferrite to austenite-finish temperature during heating (Ac_3) has been evaluated with dilatometry, and differential thermal analysis (DTA). Solid cylindrical specimens (10 mm diameter × 15 mm height) have been machined out from the as-received block in order to carry out heat treatment regimes in a Gleeble 3800® thermo-mechanical simulator. The samples have been soaked at 925-930 °C for 3-5 minutes, followed by different rates of cooling in furnace, air and water quenching. In the current set-up, the cooling rate in an excess of 10,000 °C s^{-1} can be achieved with water cooled jaw carriers fitted with an additional high-pressure quench system (0.7 MPa), pointing towards the sample cross-section from both sides. Hot deformation has been carried

out by soaking the sample in the austenitic temperature domain in 0.5 compressive strain and the strain rate 0.01/s, followed by water quenching.

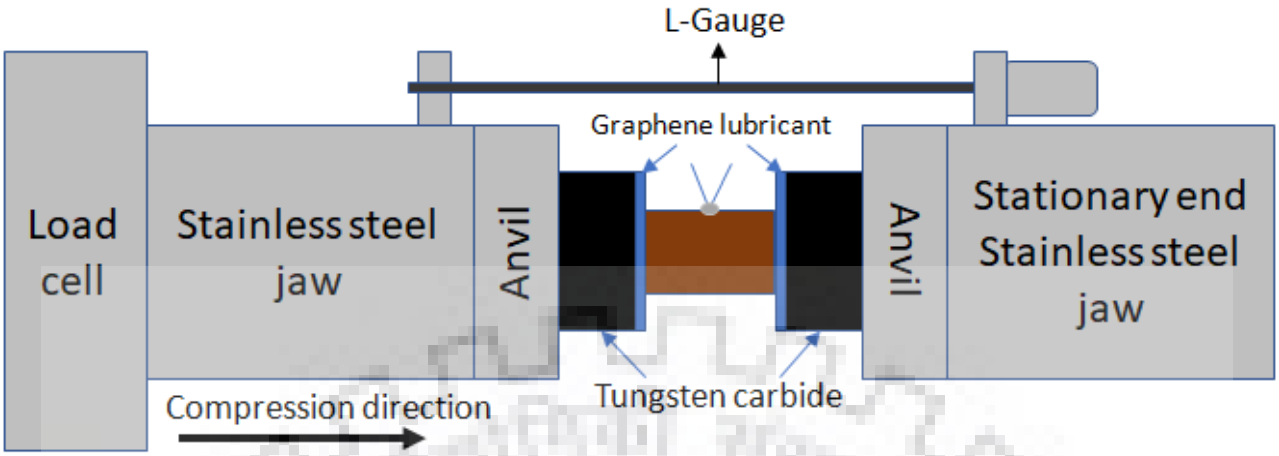

Fig. 1: The Schematic arrangement of the thermo-mechanical processing or heat treatment in a Gleeble® 3800 Thermo-Mechanical Simulator (TMS).

Microstructures have been studied from the cross sections of the heat treated samples following standard metallographic techniques, etched with 2% nital and observed under an optical microscope (Leica DMI 5000M), a field emission gun scanning electron microscope (SEM) (FEI Quanta 200 at 20 kV) with the attachment of an electron backscattered diffraction (EBSD) and high resolution transmission electron microscopy (HRTEM) (JEOL JEM 3200FS at 200 kV). For EBSD, the sample surfaces have been polished with a colloidal silica suspension (0.06 µm grade) followed by electro-polishing using an electrolyte solution of 10% perchloric acid + 90% methanol with an operating voltage of 20 V in liquid nitrogen (-30 ºC) atmosphere. A spot size of 0.2 µm and a step size of 0.3 µm have been chosen for the EBSD scan. The *TSL OIM* software has been used to interpret the scanned data. The confidence index value has been set <0.2 with a grain dilation of <0.2 for the analysis. The geometrically necessary dislocation density (ρ_{GND}) has been calculated using the equation: $\rho_{GND} = {}^{2\vartheta}/_{ub}$, where the Kernel average misorientation (KAM) values (ϑ) along with the step size of EBSD scan ($u = 0.3\ \mu m$) and the magnitude of the Burgers vector (b) of the BCC lattice have been considered. The macro-hardness of the investigated samples is measured at 1 kgf load with a dwell time of 10 s. A couple of rectangular blocks (15 × 20 × 100 mm^3) have been cut from the as-received sample and undergone same heat treatment regimes in a laboratory scale to fabricate sub-size tensile specimens following ASTM E8 standard. The tensile testing has been done with a crosshead velocity of 1 mm/minute using a Tinius Olsen system (H25 K-S at 50 KN) at room temperature.

Table 1: The chemical composition of the investigated IF steel in wt.%.

C	Mn	Si	S	P	Al	Ti	Nb	Cr	Cu	Ni	Mo	N	Fe
0.003	0.51	0.004	0.002	0.009	0.03	0.05	0.017	0.02	0.01	0.017	0.001	0.009	99.3

1.4 Work layout

In order to achieve the objectives, the overall thesis has been organized in six distinct chapters as shown in the flow-chart in Fig. 2.

	Section 1 → IF steel	
CHAPTER 1	**CHAPTER 2**	**CHAPTER 3**
Introduction, literature survey, research gap, motivation of the present work	Specimen and experimental details	Analysis of results and discussion

	Section 2 → Low density steel	
CHAPTER 4	**CHAPTER 5**	**CHAPTER 6**
Introduction, literature survey, research gap, motivation of the present work	Specimen and experimental details	Analysis of results and discussion

Fig 2: Contribution of each chapter to achieve overall objectives in the present study.

1.5 Results and discussion

The preliminary investigations suggest that the as-received sample at room temperature is ferritic with a bimodular grain-structure. The average grain size varies from 25 ± 5 μm to 240 ± 25 μm for smaller and larger ones, respectively. Fig. 5a depicts the stress-strain response of various samples. The yield stress and ultimate tensile stress (UTS) of the as-received one are 128 MPa and 199 MPa respectively and that after water-quenching increases to 391 MPa and 447 MPa, respectively with a negligible reduction in elongation from 33 to 26 pct. Thus, the result of the water-quenched (WQ) sample is the best in terms of the strength-ductility combination, compared to the annealed, normalized and as-received samples. Increasing the austenitizing temperature beyond 925 °C deteriorates the strength, while isothermal holding for 5 minutes optimises the tensile properties.

In order to analyse the tensile plots more vividly, fractography has been performed from the gauge portion of the deformed tensile samples in Figs. 3(b-e). The as-received sample shows deep dimples clearly (Fig. 3b). The depth of the dimple decreases in the annealed sample along with an increase in the number density to tailor a large elongation in Fig. 3c. In this aspect, the normalized sample shows a remarkable contrast by evidencing the formation of numerous microvoids (Fig. 3d). Besides microvoids, the WQ sample exhibits a quasi-cleavage type pattern additionally (Fig. 3e). This is an implication that a harder phase has possibly inflicted in the sample. The immediate concerns would be to study the microstructures for a relative comparison.

Figs. 3(f-h) shows the SEM micrographs of the heat-treated samples after soaking at 925 °C for 5 minutes as the optimum condition. The annealed sample under furnace cooling exhibits the initiation of fine ferrite. It signifies that during heating and soaking stages of the annealing cycle,

austenitization happens (Fig. 3f). In the case of normalizing, relatively a higher cooling rate leads to the formation of fine grains as well as lattice shearing (Fig. 3g). This particular feature can be concluded as the traces of bainite in the normalized sample which may contribute to the increment of the UTS value (Fig. 3a). In the WQ sample, a lath type of feature can be seen (Fig. 3h), and that under Le-Pera's reagent turns into straw yellow colour regions as martensite (Fig. 3i).

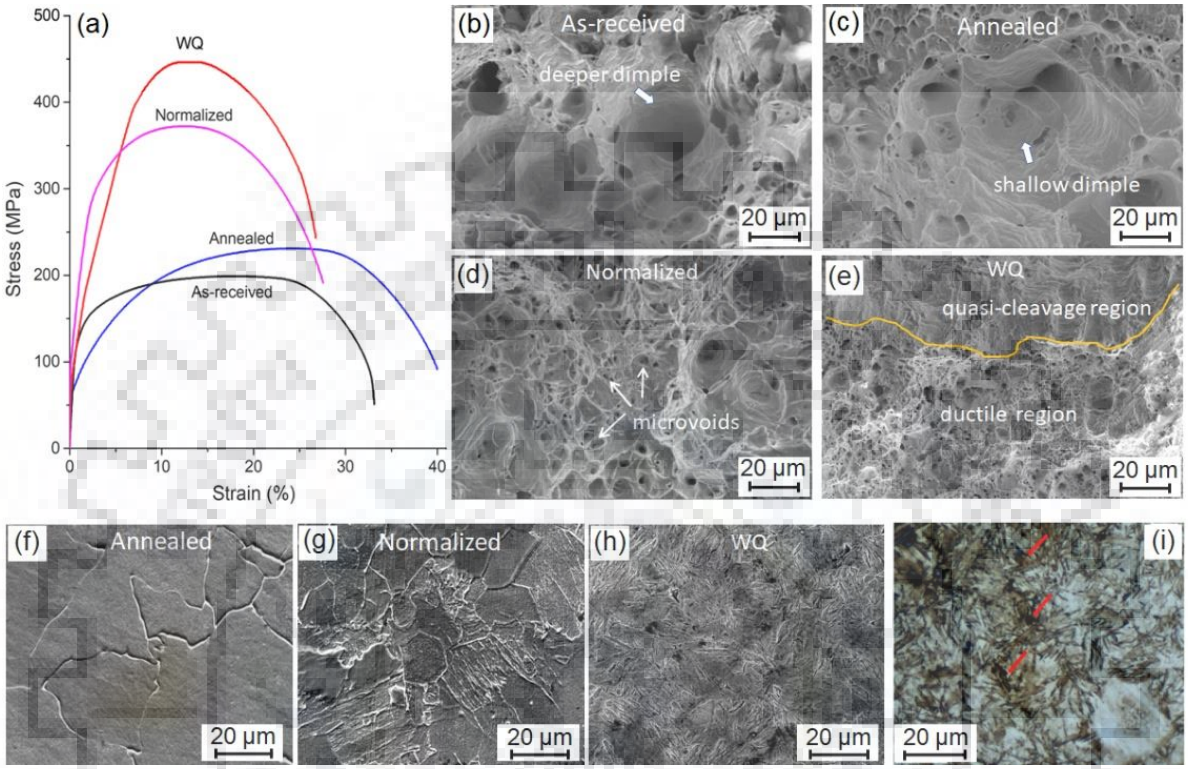

Fig. 3: (a) Engineering stress-strain curves of heat-treated samples soaked at 925 °C for 5 minutes against the as-received one. Fractographs of (b) as-received, (c) annealed, (d) normalized and (e) water-quenched (WQ) samples. SEM images of (f) annealed, (g) normalized and (g) WQ samples. (i) The WQ sample after tint etching turns into straw yellow colour selectively in the martensite regions (red arrows).

Fig. 4a shows the electron micrograph of the WQ sample under a bright field condition. Typically, the lath structure can be seen arranged parallel to each other. Under a high-resolution transmission contrast, features of lath structure become more prominent in Fig. 4b. The measured average lath thickness is near about 0.25 μm. These fine lath structures are very much indicative of a shear transformation in the investigated samples from fine prior austenite grains. In the lath regions, the formation of dislocations and its simultaneous movement producing dislocation pile-up can be seen with a dark contrast as a response of large undercooling, alleviating the internal stresses (Fig. 4b). The selected area diffraction (SAD) pattern shows that the transformed product phase is having a BCC lattice (Fig. 4c). Some twin spots are also marked by red circles in the SAD pattern, as an implication of forming the internal substructures within the lath by twin boundaries. Thermodynamic criteria can be used to discuss the feasibility of lath formation.

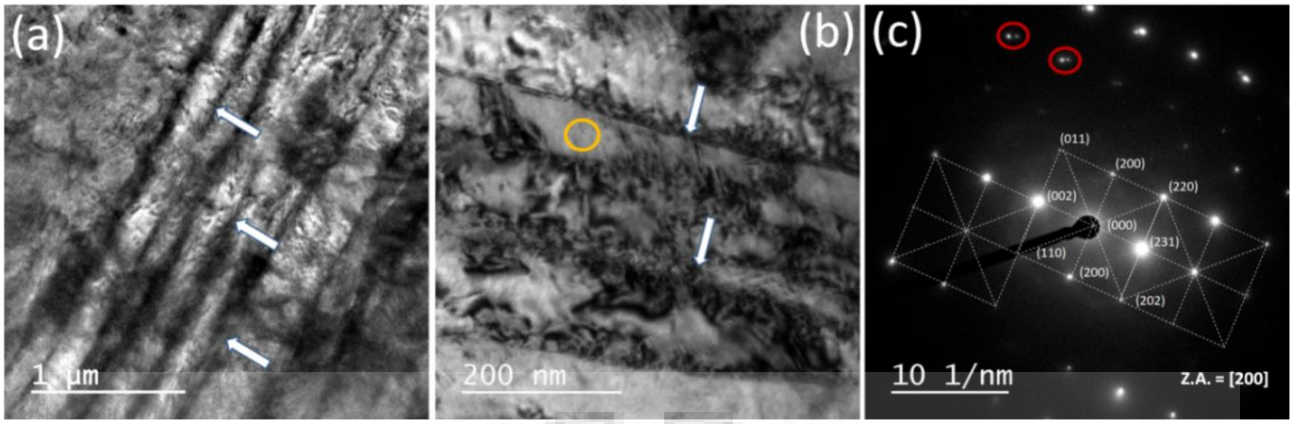

Fig. 4: Bright field (a) TEM and (b) HRTEM micrographs of the WQ sample, exhibiting lath features surrounded by dislocations (arrows). (c) SAD pattern from lath (yellow circle), showing BCC lattice with a zone axis of [200].

The equilibrium conversion of austenite to martensite (α′) is designated as T_0 temperature, where the parent and product phases of the identical composition possess equal free-energy. After rapid cooling from T_0 to M_S temperature, the changes in the crystal structure (γ → α′) happen by the diffusionless, displacive and shear mechanism. Larger the difference between T_0 and M_S, higher would be the deformation shear. According to *Thermo-calc* calculations, the T_0 temperature is about 892 °C to be within the intercritical domain of Ae_1 (880 °C) and Ae_3 (910 °C). The M_S temperature (518 °C) is closer to that one. As a result, the net difference between these two ($\Delta T = T_0 - M_S$) is 374 °C. This accounts for a net driving force of 1.1 kJ/mol approximately, as compared to a larger ΔT or driving force for high carbon steels. Thus, EBSD analysis is required to track the formation of any other phase.

The image-quality (IQ) map shows a lath type feature in Fig. 5a. In the same micrograph the presence of a granular structure can be seen, as hinted in the fractograph (Fig. 3e) and the transformation curve that the WQ sample may contain a duplex structure. The IQ map by means of the Kikuchi-pattern intensity differences provides a relatively brighter image contrast from regions of this new phase. In order to distinguish it, literature report suggests that below T_0 the early product from austenite is massive ferrite. It requires a smaller undercooling and a moderate cooling rate than that for martensite, yet inheriting the same composition of the parent austenite. The transformation is believed to occur at an interface-controlled rate. The growth is not limited by grain boundaries of the parent phase and the ability of the product crystals to cross such boundaries seems particularly pronounced in massive transformations. As a result, they do show a large variation in grain size and highly irregular grain shapes with ragged boundaries, as is clearly visible in the IQ map (Fig. 5a).

Massive ferrite is the high-temperature product of austenite. The driving force required to initiate its transformation from austenite is always much lesser than the martensitic reaction. Thus, massive ferrite appears first, followed by martensite during continuous cooling in the investigated WQ sample. The Vickers hardness (VHN) of martensite and massive ferrite in the IF steel is 236 and 118 respectively; on comparing this with the bulk (194 VHN), the duplex microstructure in Fig. 5a contains about 65% lath on the weighted average. Pascover and Radcliffe have suggested that irregular large grains of massive ferrite contain recovered sub-grains. The dislocation density

(ρ_{GND}) thus is smaller for massive ferrite (3.9×10^{14} m^{-2}) than martensite (7.9×10^{14} m^{-2}) in the current study (comparing marked regions of Fig. 5b). The point-to-point misorientation from A–B in Fig. 5c suggests that the peak value of the misorientation angle is ~60º for the lath boundaries, as compared to a minute variation by the sub-grain boundaries in massive ferrite (Fig. 5d). This eventually helps to distinguish massive ferrite from martensite; besides reinstating the fact that lattice strain/distortion is higher in martensite than massive ferrite.

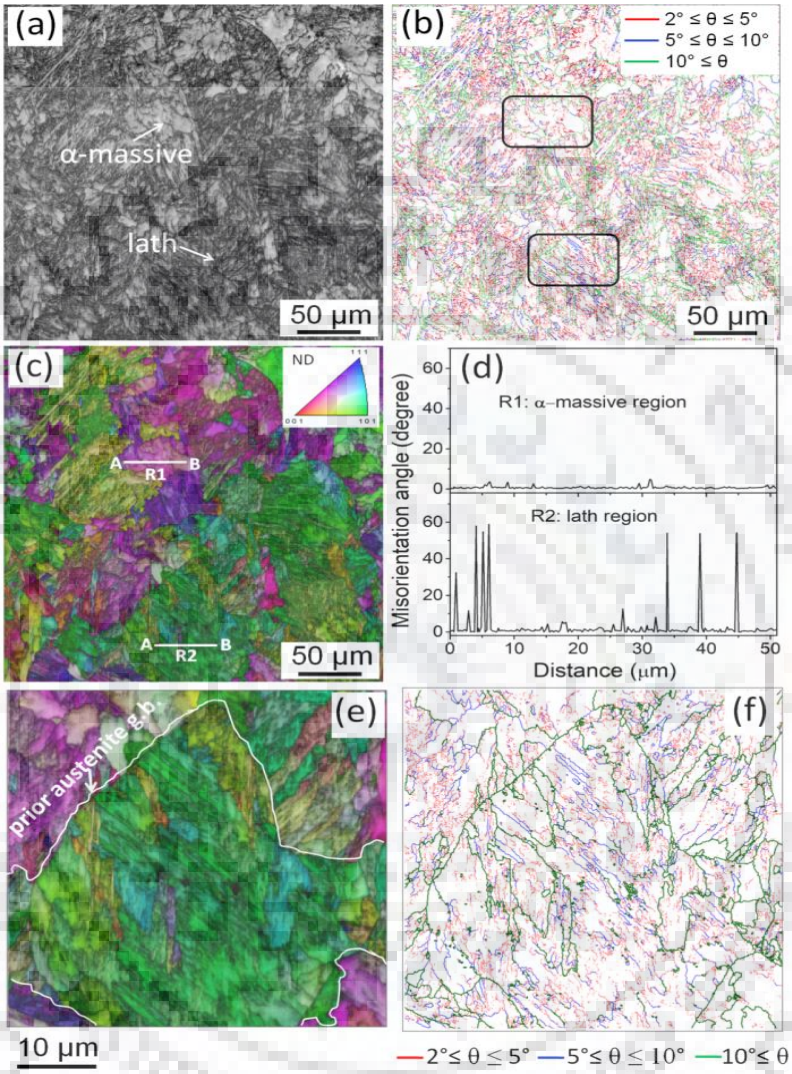

Fig. 5: EBSD analysis of WQ sample, showing (a) image quality, (b) grain boundary misorientation, (c) IPF plus IQ, (d) point-to-point misorientation angle over the distance A-B from (c). (e) (IPF + IQ) map highlighting martensite lath within a prior austenite grain and (f) the angle of misorientation from the same region.

The hierarchical microstructure of martensite consists of packets, blocks, sub-blocks, and laths within a prior austenite grain as shown by a well-defined grain boundary with a white line in Fig. 5e. The packet boundaries can be identified with the threshold value of the misorientation angle greater than 10º as depicted by green lines within the prior austenite grain in Fig. 5f. Each packet is subdivided into blocks with an angle of misorientation within 5-10º denoted by blue lines where the laths maintain a parallel alignment with each other. Further, a block contains many sub-blocks. The misorientation angle difference for the sub-block boundaries is within 3-5º as shown by red lines.

The laths within the sub-block belong to the same crystallographic variant through orientation relationships (ORs) with the parent matrix.

Phase transformation from deformed austenite: The effect of hot deformation on austenite to martensitic transformation is of the interest for some times. In ultra-low carbon or interstitial free steel, such attempt is rare. In order to execute the work, the alloy composition is kept constant, except changing the processing condition. Fig. 6a shows the scanning electron micrograph in this light (soaking the sample at 930 °C for 5 minutes, then applying 0.5 strain under compression at the strain rate 0.01/s plus water quenching). The lath type feature can be seen in the sample with green arrows. In the same micrograph, regions with orange arrows show a secondary phase of the interest for further characterization. During hot deformation of austenite, the grain boundary area per unit volume increases which in turn increases the tendency for the diffusional transformation of ferrite. The alternative sites are some special boundaries, deformation bands, etc., in the case of localized strain.

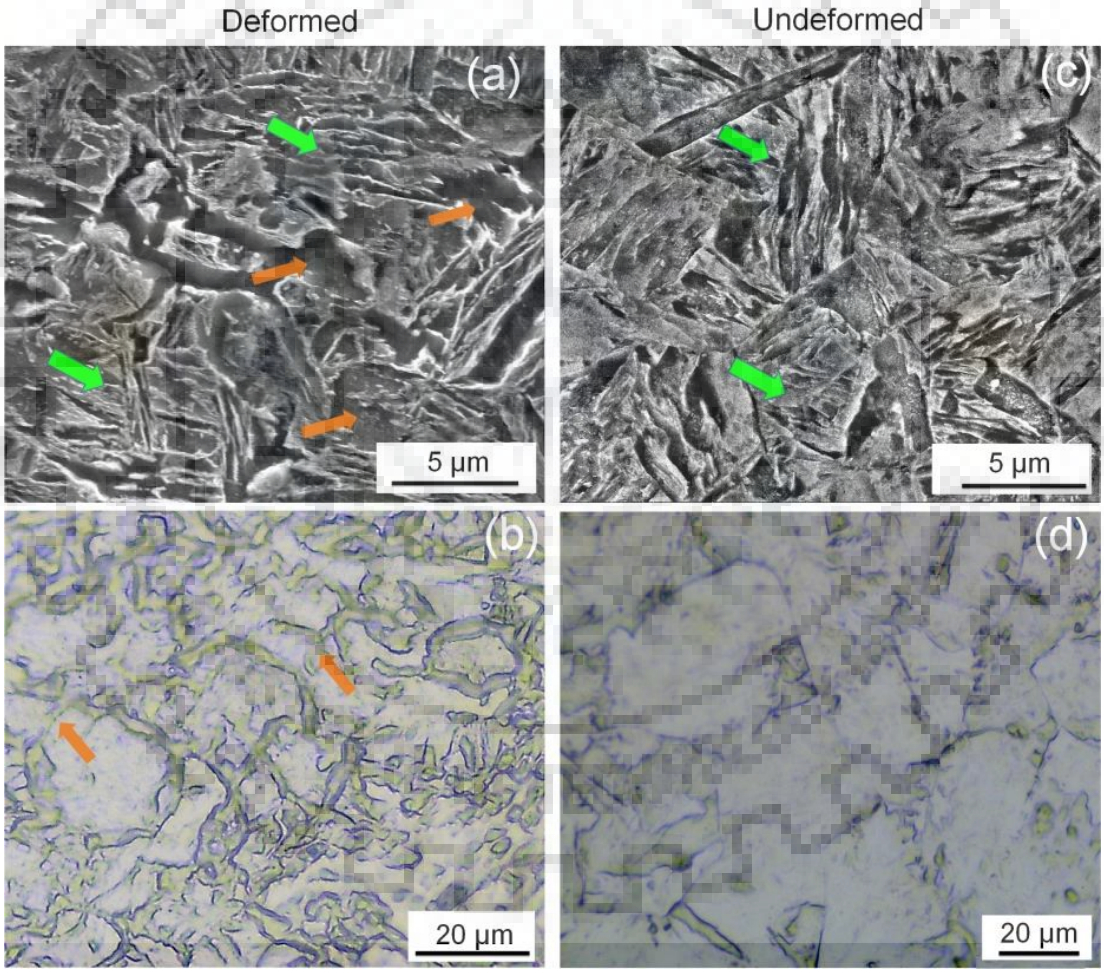

Fig. 6: (a) SEM image of the hot deformed sample, indicating diffusional ferrite and lath martensite with orange and green arrows, respectively. (b) The deformed sample after hot picric acid etching, revealing discontinuity in the prior austenite grain boundaries by the orange arrows. (c) The corresponding SEM image in the undeformed condition does not show diffusional ferrite other than lath martensite (green arrows). (d) The prior austenite grain boundaries are clearly revealed, emphasizing continuity.

The soft ductile IF steel appears to be highly malleable in the austenite phase, without cracking or deformation bands. After ensuring this, the sample has been etched with hot picric acid solution, which suppresses all the phases present other than prior austenite grain boundaries in clear details. It shows that prior austenite grain boundaries are discontinuous in some regions (Fig. 6b). The observation is consistent with the SEM micrograph, showing diffusional formation of fine ferrite within 2-4 μm sizes (Fig. 6a). The undeformed one in this respect does not provide the later phase, making the look of the grain boundary continuous (Figs. 6c-d). The average austenite grain size is 40-60 μm, as compared to relatively smaller grains (~25 μm) after hot compression (Fig 6b, d). Despite high temperature deformation, dynamic recrystallization is not obvious in the present case, because the soaking (at 930 °C for 5 min) takes place below the recrystallization stop temperature, T_{nr} (958.28 °C) predicted by the Boratto equation for the present alloy composition. In this juncture, martensite crystals are forced to nucleate at the grain interior, because austenite grain boundaries are already preoccupied by diffusional ferrite in advance. This requires overcoming a larger activation energy barrier for a solid state phase transformation; and thereby, a less martensite fraction for further scrutiny with electron micrographs.

A commercial grade of interstitial free steel with a bimodular grain structure has been thermo-mechanically processed after soaking at 925-930 ºC in the austenitizing temperature for 3-5 minutes followed by different rates of cooling in annealed (~3 ºC/s), normalized (~26 ºC/s) and water quenched (~ 730 ºC/s) conditions. Hot deformation (soaking at 930 °C for 5 min, 0.5 compressive strain, followed by water quenching) was also carried out. The engineering stress-strain curves have yielded the best combination of strength and ductility in the IF steel so far in the current water quenched (WQ) sample. The appearance of the fractrographs changes from ductile to quasi-cleavage nature accordingly with the rapid increment of the cooling rates. The computed CCT diagram has further reflected the possibility of martensitic transformation in the WQ sample. The characterization sequences are listed below to confirm martensite as the novel finding in the current system.

- The WQ sample has revealed a lath type feature in the scanning electron micrograph. With the HRTEM bright field micrographs, fine lath type of features with highly dislocated structures have been observed. In the SAD pattern, evidence of BCC product lattice has also been indexed.
- The IQ map extracted from EBSD has encountered a highly irregular grain shaped region with ragged boundaries; which in turn imparts a significant difference of image quality values compared to the lath regions in confirming massive ferrite as the duplex phase.
- The higher amount of the degree of misorientation, as well as the two-fold increment of dislocation density in the lath region, distinguishes it clearly from the massive ferrite region.
- The {100}, {110}, {111} and {112} poles from the lath region agrees with the theory to confirm martensite with different variants.
- The calculated variants on the basis of K-S orientation relationships between parent and product phase as projected in the pole figure further designate that the transformation of differently oriented martensite can originate from a single parent austenite grain. However, the maximum achievable tensile strength (UTS) is limited to 447 MPa.

- The result does not see much influence of the hierarchical structure of martensite such as block and sub-block boundaries for efficient dislocation locking, other than the packet and lath boundaries being continuous with the high angle of misorientation. In the present case, further enhancement of strength is difficult, as the number of packet boundaries is fixed by the crystallographic habit planes and the laths are refined.
- The effect of plastic deformation (50% at of 0.01 s^{-1} and 1 s^{-1}) during heat treatment at 925-930 °C in austenite domain followed by water quenching does not alter much the fraction of lath martensite. Strain induced fine precipitate of (Ti,Nb)C/N type arises in the system, but failed to incorporate additional strength.
- The maximum number of variants has been observed in the undeformed sample, as eight. After hot deformation it reduces to some extent; suggesting that constraints have intensified after hot deformation.
- The strength-ductility combination, however, remains nearly the same in both the conditions. In order to resolve the case, it appears that the deficiency of martensite during hot deformation is counterbalanced by relatively smaller austenite grains and diffusional formation of fine ferrite additionally in the system. The effect of plastic deformation incorporates some strain induced fine precipitates of the carbonitride type in the ferrite phase, but that may not alter the mechanical properties in the same scale owing to negligible in the volume fraction.
- The roles of the hierarchical structure of martensite such as block and sub-block boundaries are found to be less effective in strengthening aspects. Their discontinuous network as well as low angle of misorientation hardly can block dislocation motion, along with very fine laths also in the system.

1.6 sample details and related techniques → Low density steel

The experimental work for sample preparation is two-fold to prepare Fe-4Mn-9Al-0.3C wt.% low density steel, as the model system. In the top-down approach, first, the alloy has been prepared from the elemental blend of high purity (> 99.5%) metal powders. The process involves repeated cold welding and fracturing in a toluene atmosphere for 50 h in a Retsch planetary ball mill, employing a stainless steel jar and balls with a ball to powder ratio of 10:1 at 300 rpm. Thus, the elemental state dissolves to form a solid solution. Later the alloy powders have been compressed in an argon gas atmosphere in the spark plasma sintering (SPS) machine at 60 MPa. The application of the high pressure along with a pulsed electrical current is expected to reduce the dwell-time for the microstructure refining. In conventional sintering, heat is transferred by the radiation from a furnace wall to the powders, but in the SPS, directly at powders to be more effective. A typical heating and cooling cycle for this purpose is shown in Fig. 7a. It indicates that the temperature rise of the sample is not continuous with the time, attributed to intermediate holding at 550 °C (5 min) and 800 °C (2 min) for a better particle to particle contact over a relatively longer time, until the final temperature (1000 °C) is achieved in the multi-stage sintering. The sample porosity thus is minimized with a relative density of ~98.7% by the method of the Archimedes principle. The as-prepared sample is basically a thin pellet of the diameter and thickness of 20 mm and 5 mm respectively (Fig. 7b). In the alternative method (bottom-up approach), a green compact of ball

milled powers (~20g) has been arc melted to produce a bulk sample of the counterpart in a water cooled copper hearth of the argon gas atmosphere chamber, evacuated (10^{-5} mbar) with rotary and turbomolecular pumps.

The macro- and micro-hardness of the samples have been measured at 1 kgf and 100 g load respectively with a dwell time of 10 s for both the cases. The characterization employs X-Ray diffraction (Rigaku Smartlab), optical (Leica DMI 5000M) and a field emission gun scanning electron microscope (SEM, FEI Quanta 200) after etching the samples with 2% nital. Electron probe microanalyzer (EPMA, camera SX100) has been employed to analyze the solute distribution.

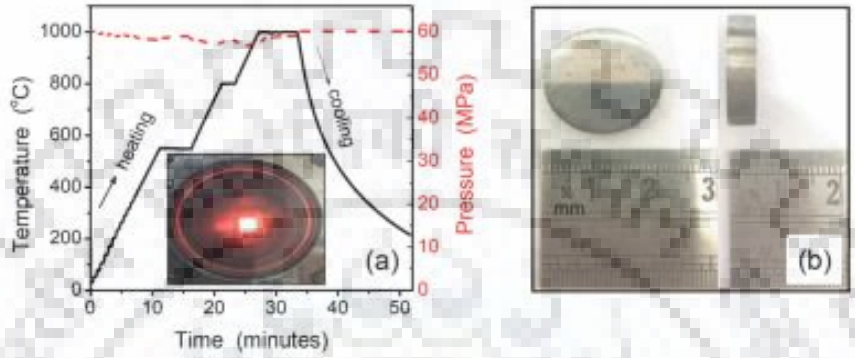

Fig. 7: (a) The illustration of the process parameters such as heating, cooling and thereby consolidation of the alloy powders at 60 MPa (dotted line) during sample preparation in the spark plasma sintering unit at the inset. (b) The sintered sample yielding a pellet of the dimension: diameter × thickness = 20 mm × 5 mm.

The sintered samples after ejection from the die have been thoroughly cleaned by chopping a few sub-layers in a grinding wheel (Fig. 7b). The Vickers hardness of the sintered sample appears to be higher (840±10 VHN) than the bulk sample (654±30 VHN). In order to understand the reason, optical microscopy has been performed. The arc melted sample exhibits a dendritic structure (Fig. 8a); whereas the sintered sample illustrates a granular type structure (Fig. 8b) until FE-SEM is performed. In Fig. 9a, the feature of the sintered sample becomes more prominent: the grain boundary like structure indeed turns out to be a porous network in the sample, and in between, a lamellar type structure can be seen as a hint of the eutectoid reaction. For details, a phase diagram calculation is necessary to understand the chemical reaction.

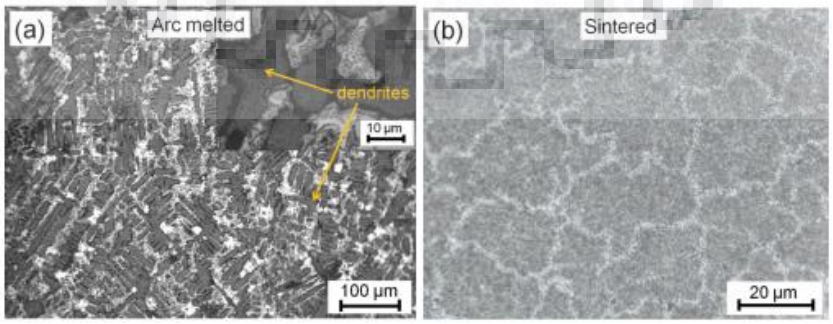

Fig. 8: The optical images, illustrating (a) dendrites in a lower and higher magnification (at the inset) for the arc melted sample, whereas (b) a granular type structure after spark plasma sintering (SPS).

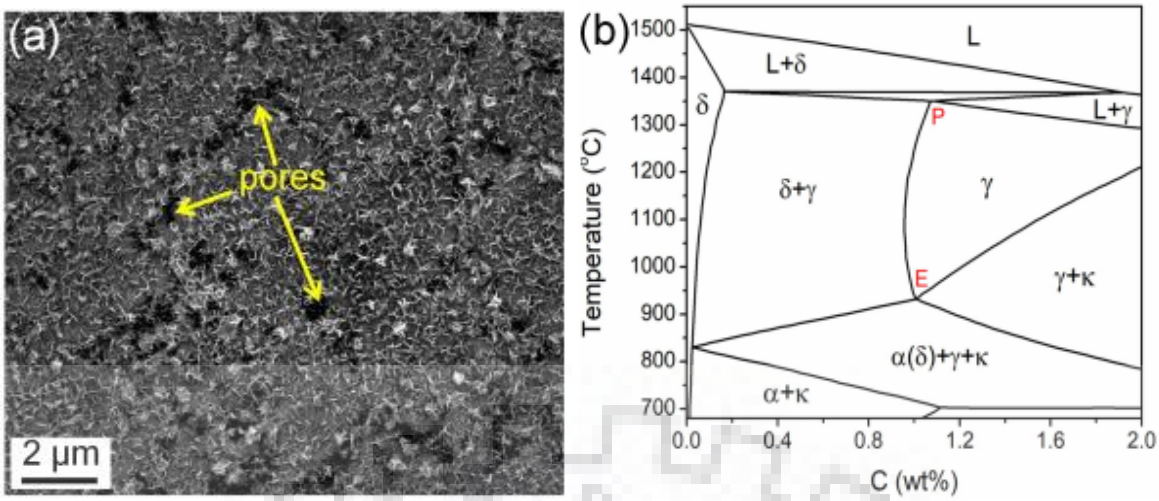

Fig. 9: (a) The FE-SEM image of the sample sintered at 1000 ℃, showing pores. (b) The phase 101 diagram of Fe-4Mn-9Al-C wt.% alloy, based on the *Thermo-Calc* calculation using the *TCFE*7 102 database.

Fig. 9b shows the computed phase diagram with the TCFE7 database, as a pseudo-binary for the convenience. It identifies two invariants at *P* and *E* to be marked as the peritectic and eutectoid points, respectively. As compared to the Fe-C binary, it shows that the peritectic reaction, which is usual in Fe-0.18%C, indeed gets shifted to 1.07% C in this multi-component system to establish the role of Al as the δ-ferrite stabilizer quite comfortably. The phase diagram further indicates that a lamellar mixture of (α+κ) from austenite is possible at 920 °C by the eutectoid reaction. The sintering temperature (1000 °C) is above this; and following which, when the alloy from the austenite regime is undercooled down to the room temperature, it passes through the κ-carbide phase domain (α(δ)+γ+κ).

Thus, the X-Ray diffraction of the sintered samples confirms the presence of α and κ in the sample in Fig. 10a. The fast diffusion of carbon and high-content of Al-partitioning are the key factors to form κ-carbide. The sintered sample with high defect density (Fig. 9a) may accelerate the diffusivity of the solute atoms, leading to the formation of κ-carbide in the present case. In this comparison, the X-ray diffraction of the arc melted sample does not show κ-carbide in the sample (Fig. 10b). The literature data as much as available suggest that the formation of κ- carbide is difficult in as-cast alloys of different alloy compositions (wt.%) as well. Gutierrez-Urrutia et al have reported that κ-carbide in Fe-30.5Mn-8Al-1.2C forms at 600 °C after 24 h annealing. Seol et al have observed κ-carbide in an Fe-0.15C-1.5Mn-4.3Al alloy only after two-step isothermal annealing: intercritical annealing at 900 °C for 30 minutes, followed by isothermal annealing at 500/600 °C for 60 minutes. Chen et al have observed an extremely high density of nano-sized κ-carbide in a water quenched Fe-8.68Al-30.5Mn-1.85C steel; but the prior history suggests that the alloy after induction melting has been homogenized at 1150 °C for 6 h, hot rolled and subsequently solution heat-treated at 1200 °C for 2 h to obtain the carbide phase. Rana et al have reported a bigger size κ-carbide in large amounts, after annealing of the aged samples. Until now, hardly there is any report of obtaining κ-carbide straightway in as- cast conditions. The present work would like to address this issue through modeling and simulation in parallel to the experiments.

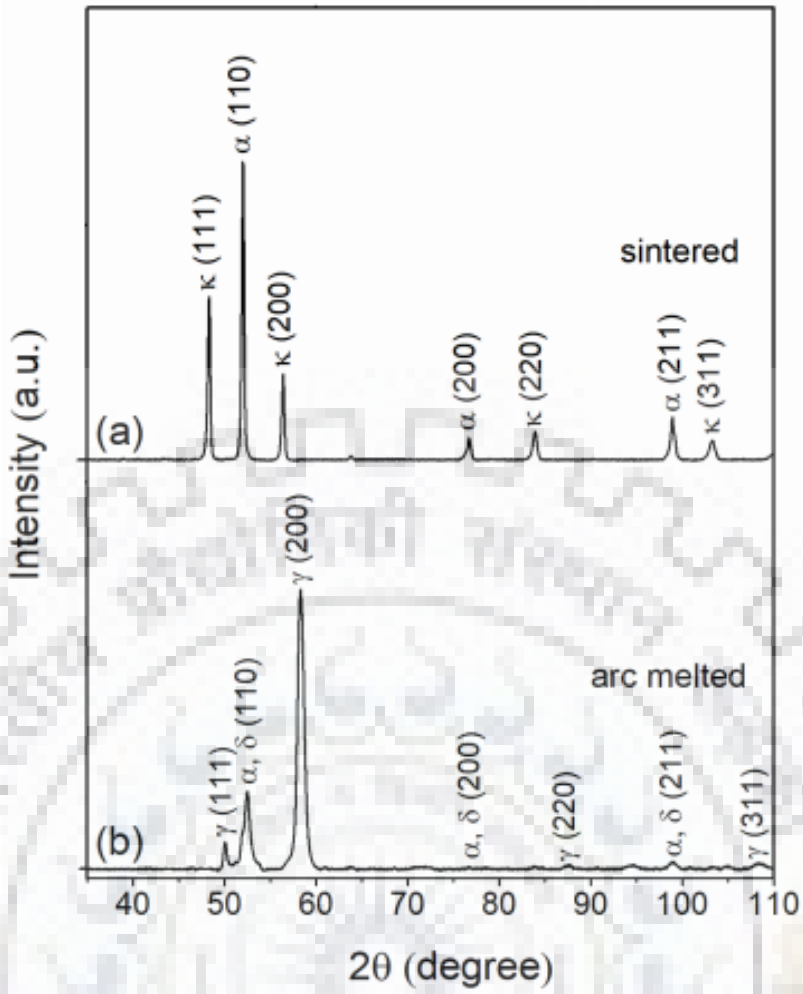

Fig. 10: The X-ray diffraction plots, exhibiting (a) the presence of κ-carbide in the sintered sample, whereas (b) absence of the later phase in the arc melted sample.

The present work has investigated phase transformation by spark plasma sintering and arc melting side by side for comparative analysis. The κ-carbide as the eutectoid product has been observed only in the sintered sample. The as-cast sample contains δ-ferrite, α-ferrite and austenite. The key reasons for the absence of κ-carbide in the as-cast sample are attributed to the following factors.

- The excessive δ-ferrite (~60%) from the liquid creates a hurdle to complete the peritectic reaction (liquid+δ-ferrite→austenite). The unutilized liquid (solute-enriched) later on gets converted to austenite directly. The formation of austenite by two different chemical reactions (peritectic- and post-peritectic) makes it inhomogeneous on the basis of the chemical composition.
- Secondly, the phase fraction of austenite in the present case is quite less (~17%), yet dissolves the majority of manganese after rejection from α- and δ-ferrite in the three phase equilibria.
- Thus, the solute-enriched inhomogeneous as it is austenite cannot undergo the eutectoid transformation (γ→κ-carbide) owing to a lack of the stoichiometry. In order to avert this, it may rather land up as retained austenite with the excess amount of manganese.
- On the contrary, the sintered samples at 1000 °C can easily bypass the formation of liquid→δ-ferrite, as well as the enrichment of manganese in austenite to ultimately resulting in uniform distribution of κ-carbide from austenite by the spark plasma sintering method.